Multiorbital and excitation effects on dissociative double ionization of CO molecules in strong circularly polarized laser fields

Xiaokai Li, Jiaqi Yu, Huiying Xu, Xitao Yu, Yizhang Yang, Zhenzhen Wang, Pan Ma, Chuncheng Wang, Fuming Guo, Yujun Yang, Sizuo Luo,* and Dajun Ding†

Institute of Atomic and Molecular Physics, Jilin University, Changchun 130012, China

(Received 4 February 2019; revised manuscript received 29 April 2019; published 17 July 2019)

We investigate the sequential double-ionization dynamics for the dissociative channel $C^+ + O^+$ of CO molecules in strong circularly polarized laser fields using four-particle coincidence measurements. By combining the fragmentation-pathway-resolved ionic angular distributions with the molecular frame photoelectron angular distributions distinguished for each ionization step, the significant effects of multiorbital ionization and laser-driven excitation are revealed. For the main distribution of ionic fragments in the polarization plane, the participation of the highest-occupied molecular orbitals (HOMO, HOMO-1, and HOMO-2) and the important contribution of postionization excitation are identified for various fragmentation pathways. Comparisons among different intensities further indicate the dependence of the multiorbital ionization on laser intensities. For the substantial emissions of fragments out of the polarization plane, however, the ionization from HOMO-1 (and subsequent excitation) always plays a crucial role. This work demonstrates the feasibility of disentangling the complex dynamics in molecular dissociative double ionization with the angular streaking method.

DOI: 10.1103/PhysRevA.100.013415

I. INTRODUCTION

Multielectron dynamics have attracted much attention in studies of the interactions of strong laser fields with atoms and molecules, such as field-induced tunnel ionization, high-harmonic generation, double ionization, dissociation, and Coulomb explosion [1–4], in order to obtain a deep understanding of the responses of multielectron systems in strong fields and to further achieve their potential applications. For molecular ionization and subsequent fragmentation, specifically, multiorbital effects have been definitely verified, where the direct strong-field ionization (SFI) from multiple molecular orbitals populates the cation in its electronic ground or excited state and initiates attosecond electronic dynamics in molecules [1,4–7]. Measuring the ionization angular distribution in the molecular frame is a useful method for distinguishing the multiorbital contributions, because the angle-dependent ionization yield is determined by the electron density distribution of specific molecular orbitals [8]. One widely employed method measures the alignment-dependent ionization or dissociation yield using aligned or oriented molecules [9–13]. Another way to determine the molecular frame angular distribution of ionization probability is, when the axial recoil approximation is sufficiently valid, to detect coincidentally the momentum vectors of electrons and ionic fragments from dissociative ionization and thus reconstruct the resulting molecular frame photoelectron angular distributions (MFPADs) [1,4,14]. For the same dissociative ionization *channel*, which produces a certain set of final fragment and electron products, the interaction of molecules with laser fields proceeding through different *pathways* of ionization, excitation, and dissociation can produce fragments with distinct kinetic energies or angular distributions. Over the past decade, many studies have investigated the different multiorbital ionization origins for distinct fragmentation pathways in the dissociative single ionization of HCl, O_2, CO, CH_3X (X = Cl, Br, I), C_4H_6, C_4H_8, C_4H_{10}, etc. [1,4,7,15–19]. It is noteworthy that, besides the SFI from lower-lying orbitals that directly populates the resulting cation in its excited state, sequential postionization excitation, following SFI to the cationic ground state, can also contribute significantly to the production of an excited molecular cation and its subsequent fragmentation [17,20,21]. This type of sequential multiphoton excitation has been observed in many experiments investigating the molecular fragmentation in strong laser fields [1,20,21], including the extensively studied electron localization dynamics in H_2^+ [22]. The contribution of sequential excitation has proven to be related to the energy gaps between the ground state and the excited states of the cation and to the photon energy of the ionizing laser. Sequential excitation contributes little when the photon energy exceeds the energy gap, and its contribution significantly increases when more photons must be absorbed for excitation [17].

To assign multiple participating ionization pathways in dissociative double ionization, some researchers have attempted to disentangle the complex ionization, excitation, and dissociation dynamics of diatomic and polyatomic molecules. The involvements of lower-lying valence orbital ionization and laser-driven excitation in linearly polarized laser fields have been revealed by detecting the isotropic or anisotropic distribution of the ionic fragments and calculating the molecular potential energy surfaces [6,23]. However, it is still a challenging task for experiments to probe the angular ionization distribution in the molecular frame to identify the ionization

*luosz@jlu.edu.cn
†dajund@jlu.edu.cn

pathways and the associated molecular orbitals in strong-field double ionization, where the two detected electrons are usually difficult to distinguish, except for sequential double ionization in circularly polarized laser fields, which can produce two electrons with separated momentum distributions [24]. Recently, the angular streaking method that has been used to measure the MFPADs of dissociative single ionization by a near-circularly polarized laser has also been extended to studies of the double-ionization dynamics of molecules in strong laser fields [4,14,25,26]. This method has the advantages of reducing the influence of postionization alignment and suppressing recollision processes in the laser fields. For instance, Winney *et al.* have measured the recoil-frame electron momentum distribution and have demonstrated that three kinds of ionization sequences from the molecular orbitals—including the highest-occupied molecular orbital (HOMO)-1 and doubly degenerate HOMOs—can contribute to the dissociative double ionization of CH_3I [14]. They have also used the same method to study electron-electron correlations and multiorbital ionization during the double ionization of C_6H_6 molecules [25,27]. In addition, utilizing the effect of angular streaking, Wu *et al.* have measured the sum of the momenta of ions, caused by the recoil from the momenta of electrons, to acquire the asymmetries of ionization probability along the molecular axis for the two sequentially emitted electrons and, hence, to analyze the contribution of lower-lying orbitals to the various fragmentation pathways of the dissociative double ionization of CO [4]. For the $C^+ + O^+$ channel produced in an elliptically polarized field with an ellipticity of 0.7 and an intensity of 2×10^{15} W/cm^2, they identified two sequential ionization pathways: removal of two electrons from the HOMO-1 and HOMO, respectively, leads to low-kinetic-energy-release (low-KER) signals, while high-KER dissociation originates from sequential removals of the HOMO and HOMO-2 electrons [4]. Though the sequential postionization excitation possibly involved in the molecular double ionization were not investigated in these works, a method including the identification of the ionized molecular orbitals and, further, the dication (pre)dissociative states related to the fragmentation pathways actually has the potential to reveal the contribution of field-driven excitation. Moreover, this method is normally performed in a circularly polarized field and can consequently avoid the disturbance from recollision-induced excitation. On the other hand, sequential postionization excitation has proven to be very important in many strong-field phenomena, such as charge-resonance-enhanced ionization or localization dynamics in H_2^+ [22,28], nitrogen ion lasers generated in femtosecond laser filamentation [29,30], and generation of neutral Rydberg fragments [31]. Therefore, to increase the understanding of the complex process of strong-field molecular physics, it is essential to disentangle the ionization, excitation, and dissociation dynamics.

In this work, we have chosen CO, one of the simplest polar molecules, as an exemplary system and performed a four-particle coincident measurement to investigate its sequential ionization and excitation dynamics in dissociative double ionization. The ground-state electronic configuration of CO is $(1\sigma)^2(2\sigma)^2(3\sigma)^2(4\sigma)^2(1\pi)^4(5\sigma)^2$, i.e., its highest-occupied molecular orbitals are composed of two σ-type (HOMO, HOMO-2) and one doubly degenerate pair of π-type (HOMO-1) orbitals [32,33], as displayed in Fig. 1(c). The energies for ionizing the HOMO, HOMO-1, and HOMO-2 of CO and CO^+ are, respectively, (13.82 and 26.99 eV), (16.74 and 27.98 eV), and (19.64 and 29.78 eV) [32]. Lower molecular orbitals are not considered here because of their much higher ionization energies.

In detail, by coincidentally measuring the KER or fragmentation-pathway-resolved angular distribution of ion fragments and the MFPADs for the sequential double ionization of CO molecules with the angular streaking method, we find clear evidence of multiorbital effects in the significant distributions of ions out of the polarization plane, the obvious contrast between the fragmentation pathways in the total MFPADs, and the distributions of the relative emission angle between electrons. As mentioned above, the pioneering study by Wu *et al.* has found the participation of electron removals from the HOMO-1 and HOMO-2, by measuring the sum of ion momenta as an equivalence of the electron momenta sum [4]. But here, with the fact that the magnitude of the electron momentum follows the envelope of the laser pulse [24], the release sequence of the two electrons can be distinguished and therefore the separated MFPADs for the first- and second-emitted electrons are obtained. The measurements at different laser intensities further indicate the intensity-dependent multiorbital effect. Moreover, by combining the MFPADs with the identification of dication states, we reveal the important role of laser-driven excitation for the different fragmentation pathways in dissociative double ionization of CO.

II. EXPERIMENTAL METHOD

Our experiments use a reaction microscope of cold target recoil ion momentum spectroscopy (COLTRIMS) [34,35] to detect coincidentally the photoions and photoelectrons produced at the intersection of focused circularly polarized laser pulses with a supersonic CO (10% seeded in He) gas jet, as shown schematically in Fig. 1(a). The ellipticity of the laser pulses obtained from a titanium-sapphire chirped-pulse laser amplifier system (800 nm, 1 kHz, ~40 fs) is adjusted to be ~0.95 by a combination of a half-wave plate and a quarter-wave plate. The resulting ions and electrons are guided to two time- and position-sensitive microchannel plate and delay-line detectors, respectively, by weak homogeneous electric and magnetic fields. The three-dimensional momentum vectors of these charged particles are calculated by the time and position information recorded from the detectors. Because the setup has a higher resolution for measuring the time of flight (TOF) than the position, detection of the ionic momentum vector generally has the highest resolution along the TOF direction [z axis; see Figs. 1(a) and 1(b)]. Meanwhile, resolution of the measured ionic kinetic energy decreases as the KER increases due to kinetic energy is in proportion to the square of the momentum. This leads to the observation of well-separated KER peaks, which corresponds to vibrational progression of the electronic state, only around the z axis and, especially, the low-KER region P1, as shown in Fig. 2(d). More details of the experimental setup can be found in our previous publications [36,37]. By adjusting the flux of the gas jet with two sets of slits, the rate of electrons is controlled to be about 0.2 per pulse to keep the false coincidence rate sufficiently

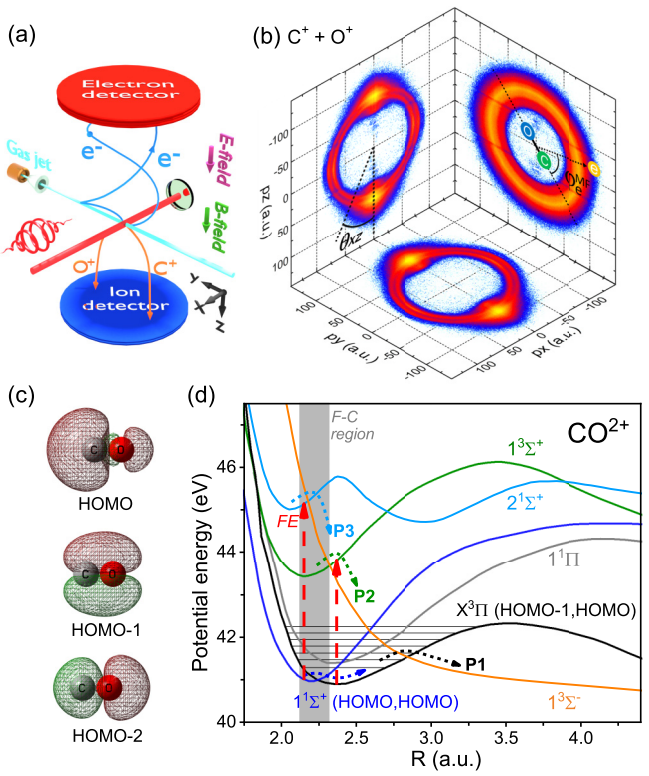

FIG. 1. (a) Schematic of the experimental setup. The polarization plane of the laser field lies in the yz plane. (b) Ionic momentum distribution projected in three orthogonal planes for the $C^+ + O^+$ channel of dissociative double ionization of CO by circularly polarized laser pulses (800 nm, 1.0×10^{15} W/cm^2). The data in each plane are from a $\pm 20^\circ$ slice parallel to the corresponding planes. The definitions of θ_{xz} and φ_e^{MF} are also shown. θ_{xz} is the relative angle between the directions of ion emission and the z axis in the xz plane. φ_e^{MF} represents the relative angle between the emission direction of the C^+ ion and electron in the polarization plane. (c) Molecular orbitals involved in this experiment. (d) Relevant potential curves of the CO^{2+} ion, adapted from Ref. [41]. Dashed red arrows denote field-driven excitation (FE). The fragmentation pathways for three KER peaks are also schematically shown.

low. To select coincidentally the two ions and two electrons produced in the dissociative double ionization of CO, only events that meet the condition $|p_{z,\mathrm{ion1}} + p_{z,\mathrm{ion2}} + p_{z,\mathrm{electron1}} + p_{z,\mathrm{electron2}}| < 0.6$ a.u. are filtered. Moreover, there is still one kind of false-coincidence event that includes the particles originating from two different ionized molecules in the same pulse. In our case of four-particle coincidence measurement, its probability is estimated in the range of 30% to 35%. By selecting the data outside the above range of momentum condition, the relevant false-correlated spectra can be generated. Further subtracting them from the original ones, we obtain the final spectra with false coincidence being largely suppressed [38,39]. The peak intensity of the laser pulse is estimated by measuring the yield ratio of Xe^{2+} to Xe^+ as a function of the pulse energy [40].

III. RESULTS AND DISCUSSION

In the experiment, we observed three kinds of double-ionization channels for the CO molecule following SFI, i.e., the nondissociative ($CO \rightarrow CO^{2+}$), charge-symmetric dissociative ($CO \rightarrow C^+ + O^+$), and charge-asymmetric dissociative ($CO \rightarrow C^{2+} + O$) channels. Their branching ratios to the total double-ionization events are 2%, 86%, and 12%, respectively (at the intensity of 1.0×10^{15} W/cm^2). In this paper, we concentrate on identifying the double-ionization and fragmentation dynamics of the charge-symmetric dissociative channel. Previous studies of diatomic and polyatomic molecules have shown that ionization from π-type orbitals can produce ions that emit out of the laser electric field polarization direction or plane [6,9,23]. In order to reveal the participation of π-type orbitals, Fig. 2(a) shows the KER-dependent ionic angular distribution for the $C^+ + O^+$ channel in the xz plane, which is perpendicular to the polarization plane (yz plane) of the circularly polarized laser fields. While the ions emit mainly near the polarization plane ($\theta_{xz} = 0^\circ$ or $\pm 180^\circ$), significant and quite homogeneous distributions also appear out of the polarization plane for specific KER regimes (P1 and P2). Three dominant KER peaks, P1 (5.1–6.2 eV), P2 (6.7–8.0 eV), and P3 (8.1–9.3 eV), are displayed in the angle-integrated KER distributions in Fig. 2(b), which includes the KERs for all ions (black line), for ions in the polarization plane (red line), and for ions out of the plane (pink line). For comparison, the normalized angular yields of the three major KER peaks are plotted in Fig. 2(c). The angular distributions for the three KER regimes have two kinds of maxima, which are located, respectively, in directions parallel to the polarization plane ($\theta_{xz} = 0^\circ$ or $\pm 180^\circ$) and perpendicular to the polarization plane ($\theta_{xz} = \pm 90^\circ$). These maxima imply that multiple pathways should be involved in the production of the same KER peak. Among them, the maxima appearing at $\pm 90^\circ$ suggest important contributions from the HOMO-1 π-type orbital to the two major peaks P1 and P2, similar to the case of C_2H_2 [26]. As an aside, the charge-asymmetric channel $C^{2+} + O$, which has two distinct peaks in the total KER distribution (at 2.0 and 2.9 eV; not shown here), has strong distributions only in the polarization plane [dotted orange line in Fig. 2(c)]. This suggests that this channel originates from ionizations dominated by σ-type orbitals, similar to a proposal for the charge-asymmetric dissociation of N_2 [42].

To discover more details about the multiorbital ionization and excitation pathways, we have further filtered the events with the ions emitted in the polarization plane to reconstruct the MFPADs. Though the total MFPAD for the two electrons from dissociative double ionization has been measured in previous works [14,26], distinguishing the MFPAD for each single ionization step, which is meaningful and desired, has rarely been studied. In a study of timing the release of each of the two electrons emitted sequentially from argon, Pfeiffer *et al.* have demonstrated that the magnitude of the electron momentum in the polarization plane follows the envelope of the laser pulse, and they were thus able to distinguish the electrons that were released during the first and second ionizations [24]. In our experiment, the high laser intensities employed here (in the range of 0.75 to 1.5×10^{15} W/cm^2) lie clearly in the regime of sequential double ionization for CO molecules, as many other atoms and molecules with similar ionization energies [44,45]. And the circularly polarized laser pulses we applied are able to suppress strongly the recollision-induced nonsequential double ionizations. Hence, it is reasonable here

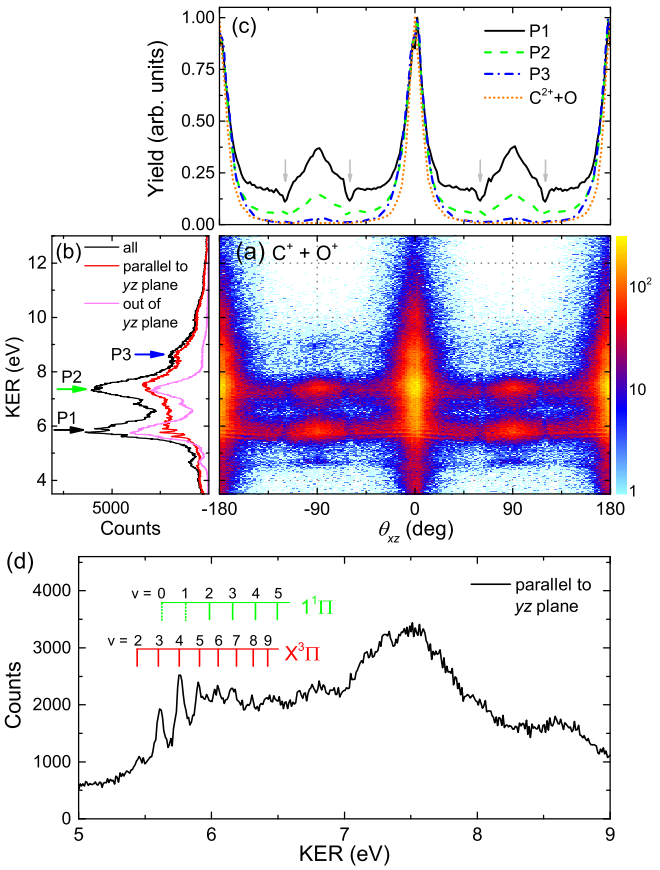

FIG. 2. (a) KER-resolved ionic angular distribution for the dissociative double ionization ($C^+ + O^+$) of CO at 1.0×10^{15} W/cm^2. (b) Angle-integrated KER distributions for the emission angles of all the ions (solid black line), for those parallel to the polarization plane (within the range of $\theta_{xz} = 0^\circ \pm 20^\circ$ or $180^\circ(-180^\circ) \pm 20^\circ$; red line), and for those out of the polarization plane (within the range of $\theta_{xz} = 90^\circ(-90^\circ) \pm 70^\circ$; pink line), respectively. (c) Normalized KER-dependent ionic angular distributions for the three distinct fragmentation pathways P1 (solid black line), P2 (dashed green line), and P3 (dash-dotted blue line), respectively. The same angular distribution for the charge asymmetric dissociation is also shown (dotted orange line). For these spectra, we chose ions parallel to the xz plane within the angle range of $\pm20^\circ$. (d) Enlarged KER spectra for ions emitted parallel to the yz plane, i.e., along the z axis (TOF direction). KERs corresponding to the vibrational progressions of the $X\,^3\Pi$ and $1\,^1\Pi$ states are taken from Ref. [43] and have been offset with a decrease of 0.22 eV. Gray arrows in (c) indicate the low efficiency for detecting two ions with identical TOFs induced by the deadtime of the detector.

to separate the two electrons by the absolute values of their momentum vectors in the polarization plane for every single measured double-ionization event. These absolute values of momenta are determined by their coarse ionization time, namely, by the amplitude of the electric field at the rising edge of the pulse envelope when the electrons are released [24]. The resulting molecular frame photoelectron momentum spectra coincided with the three major KER peaks (P1, P2, and P3) are presented in Fig. 3, with the spectra for the first-emitted electron shown in Figs. 3(a)–3(c) and the spectra for the second-emitted electron shown in Figs. 3(d)–3(f). C^+ ions are rotated

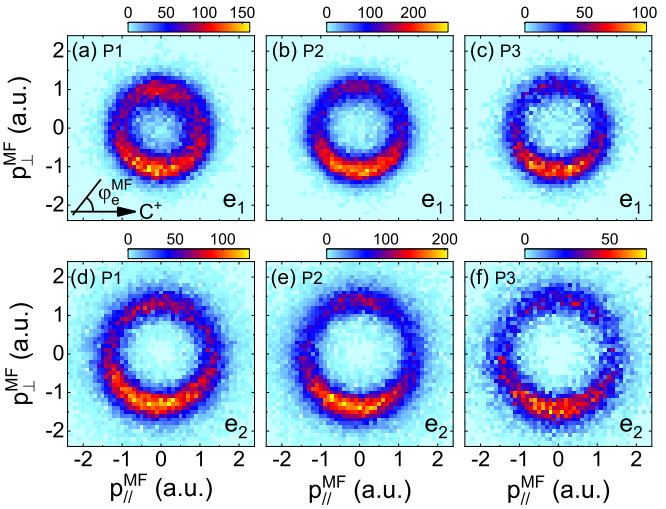

FIG. 3. Molecular frame momentum spectra of the first (a–c) and second (d–f) electrons (labeled e_1 and e_2) coincide with the ions from, respectively, the KER peaks of P1, P2, and P3 for the $C^+ + O^+$ channel at 1.0×10^{15} W/cm^2. To reconstruct the molecular frame spectra, we chose events with ions emitted in the polarization plane over the range of angles $\pm20^\circ$. Angular streaking induces the deflection angle of $\sim90^\circ$ between the electron momentum and the molecular axis.

to the same direction to reconstruct the molecular frame. The deflection angle of $\sim90^\circ$ between the directions of the departing electron and the molecular axis is induced by the angular streaking effect in circularly polarized laser fields [46–48]. The measured results in Fig. 3 suggest that the momenta of the second electrons are generally higher than those of the first electrons, which also demonstrates the validity of this identification method.

With the help of the separated MFPADs, the multiple orbitals involved in the molecular double ionization can be identified for each ionization step. Comparing the molecular frame momentum spectra shown in Fig. 3 qualitatively, we find that the momentum distribution of the first electron from P1 [Fig. 3(a)] is more homogeneous than the others. This difference is also observed obviously in the correlated MFPADs of the two electrons, as marked by the dashed yellow circles in Fig. 4(a), except that the correlated MFPADs in Figs. 4(a)–4(c) exhibit similar structures. The major bright blocks around $(-100^\circ, -100^\circ)$ indicate that the electrons released by the sequential double ionization are emitted mostly from the C side of the CO molecule. The minor distributions around $(90^\circ, -100^\circ)$ and $(-100^\circ, 90^\circ)$ represent two electrons emitted from opposite sides of the molecule. The offset about $\sim10^\circ$ in the maximum angular distribution of electrons emitted from the C and O sides may be induced mainly by the different effects of the Coulomb potential [46,49] on the electrons escaping from different ends of the polar molecule. And few distributions are observed around $(90^\circ, 90^\circ)$, where both of the electrons are emitted from the O side. This observation is consistent with the sequential double-ionization scenario for polar molecules. To permit quantitative comparisons, we plot the normalized MFPADs of the first and second electrons in Figs. 4(d)–4(f). The dashed blue and dotted cyan curves in

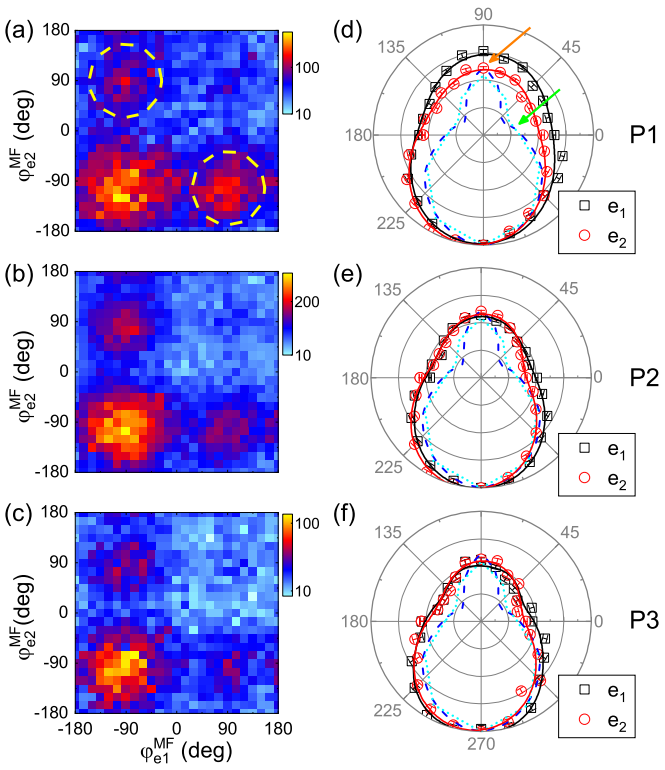

FIG. 4. (a–c) Molecular frame angular correlations and (d–f) angle-dependent ionization yields for the first and second electrons in coincidence with the KER peaks P1 (a, d), P2 (b, e), and P3 (c, f), respectively. Dashed blue and dotted cyan lines in (d–f) show, respectively, curves fitted to the measurements of, and the results calculated for, the molecular frame photoelectron angular distribution ionized from the HOMO of CO, adapted from Refs. [4] and [33].

these figures represent MFPADs for SFI from the HOMO of CO, adapted from Refs. [4] and [33]. The former is a curve fitted to the measured MFPAD obtained from dissociative single ionization of CO by circularly polarized laser pulses [4]. The latter is the ionization yield from 5σ electrons calculated by three-dimensional time-dependent Hartree-Fock theory [33]. As shown in Figs. 4(d)–4(f), all the other measured electrons have similar angular distributions that agree well with the reference curves, except for the first electron from P1 [marked by the orange arrow in Fig. 4(d)]. This is especially true for the ratio of the two peak values, which can reflect the profile of the involved molecular orbitals [4]. Considering that the angular distribution for the photoelectron emitted from HOMO-1 has a quite small asymmetry between the two extreme values, as illustrated in Ref. [4], the MFPAD for the first electron from P1 in the present work, whose asymmetry actually lies between the HOMO and the HOMO-1 cases, can be explained by ionization from both of these orbitals of CO. As for the MFPADs of other electrons, the good agreement of their asymmetries with the reference curves suggests that these electrons are emitted predominantly from the HOMO. By the way, the decreasing difference between our measurement and the reference curves around 0° [marked by the green arrow in Fig. 4(d)] as the KER increases from P1 to P3 may be induced by a decreasing contribution from HOMO-1 ionization, for which the electron density is dominantly distributed perpendicular to the molecular axis. This decrease is actually in accordance with the descending yield of the ions emitted out of the polarization plane from P1 to P3 [pink line in Fig. 2(b)].

By combining the above-identified molecular orbitals with the following distinguished (pre)dissociative states of dication associated with the fragmentation pathways, the intermediate process taking place between ionization and dissociation can be inferred, such as field-induced excitation and indirect predissociation. As CO is a simple but typical heteronuclear diatomic molecule, its KER spectra that were obtained from dissociative double ionization produced by electron collisions or synchrotron radiation and from theoretical CO^{2+} potential energy curve calculations have been extensively studied. These works show that the three major KER peaks we observed can be produced by coupling the dicationic states $X\,^3\Pi$ ($1\,^3\Pi$, $1\pi^{-1}\,5\sigma^{-1}$), $1\,^1\Sigma^+$ ($5\sigma^{-2}$), $1\,^1\Pi$, $1\,^3\Sigma^+$ ($4\sigma^{-1}\,5\sigma^{-1}$), and $2\,^1\Sigma^+$ to the repulsive $1\,^3\Sigma^-$ state [41,43,50]. These states are the lowest electronic states of the CO dication and thus have the largest populations. The former three states have overlapping energy release spectra extending from 5.6 to as high as 7.5 eV, and the other two states result in KERs of about 7.8 and 9.5 eV [43], corresponding to the KER peaks P1, P2, and P3 in this work, respectively. We note that the KERs in the present work are slightly smaller than some previous results by electron collision [41,43] or strong-field laser pulses [4] but similar to some other measurements in strong laser fields [51]. In fact, the KER of strong-field-induced dissociation is related to the parameters of the laser pulse, such as the intensity and pulse chirp [52–54]. This difference actually would not affect our identification of the (pre)dissociative states. Figure 2(d) shows the KER distribution along the TOF direction and well-separated peaks associated with vibrational states can be observed clearly for P1. These peaks fit well with the KER peaks obtained by electron collision (with an offset of −0.22 eV) [43], which corresponds to the vibrational progressions of the $X\,^3\Pi$ and $1\,^1\Pi$ states. Thus, it demonstrates that P1 results mainly from the predissociation of the $X\,^3\Pi$ states (the $1\,^1\Pi$ states not contribute much). On the other hand, according to Koopmans' picture [6,17], the $1\,^1\Sigma^+$ state is populated after the sequential release of two electrons from HOMO, while the $X\,^3\Pi$ state corresponds to the removal of one electron from HOMO-1 and the other electron from HOMO. Therefore, the MFPADs associated with P1 suggest that both the $1\,^1\Sigma^+$ and the $X\,^3\Pi$ state, populated after the removal of two electrons, contribute to the production of P1. This contradiction can be explained by the indirect predissociation of the $1\,^1\Sigma^+$ state. From calculations of spin-orbit interaction, Šedivcová *et al.* [50] have shown that, although both the $1\,^1\Sigma^+$ and the $X\,^3\Pi$ states are coupled to the $1\,^3\Sigma^-$ state, the excited $1\,^1\Sigma^+$ state mainly decays indirectly through the $X\,^3\Pi$ state because of the mixing between them and then predissociates by the coupling with the $1\,^3\Sigma^-$ state, as shown by the dotted blue and black arrows in Fig. 1(d). Hence, we disentangle the ionization and predissociation process for the low-KER peak P1 and identify two pathways for its production, including multiorbital ionization from HOMO and HOMO-1.

However, for the high-KER peaks P2 and P3, it is found that the influence of field-induced excitation should be considered at the lower intensities and that multiorbital

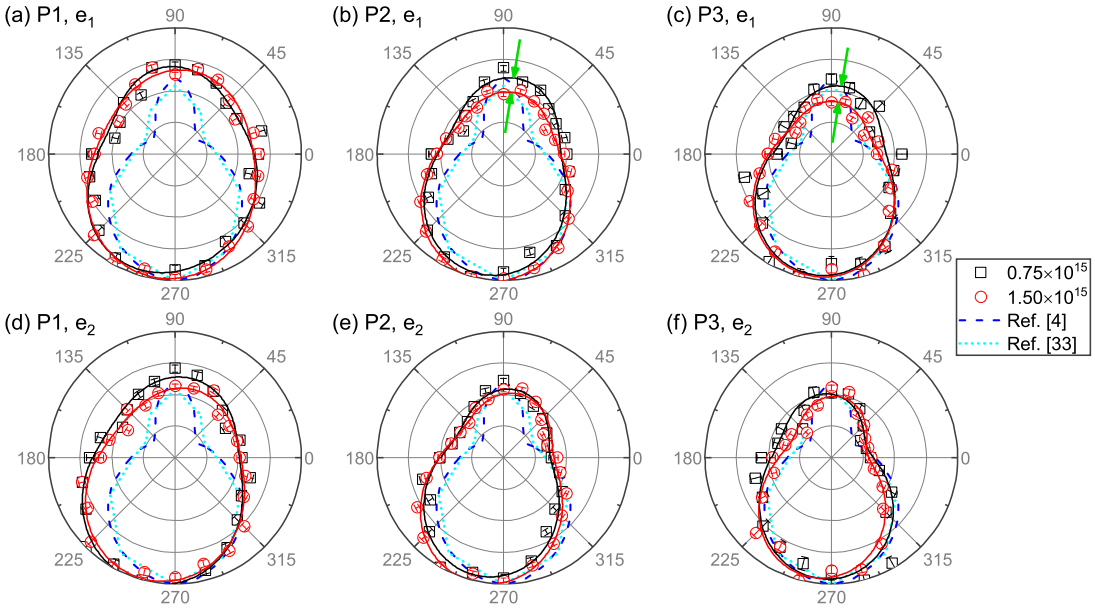

FIG. 5. Comparison of molecular frame angular ionization yields for the two electrons coinciding with three distinct KER peaks for laser intensities of 0.75×10^{15} (black squares) and 1.5×10^{15} W/cm^2 (red circles).

ionization depends on the laser intensity. Figure 5 shows the MFPADs (corresponding to the same KER regions as in the above discussion for 1.0×10^{15} W/cm^2) measured at two other intensities, 0.75 and 1.5×10^{15} W/cm^2. One can see that the asymmetries along the molecular axis for the first ionization of P2 and P3 obtained at 1.5×10^{15} W/cm^2 are obviously larger than those obtained at the lower intensities [marked by green arrows in Figs. 5(b) and 5(c)], while the other asymmetries are generally similar at all three intensities. This observation, which contradicts the expectation of a more isotropic angular distribution resulting from ionization saturation or depletion, suggests that ionization saturation or depletion should have little influence on the measured angular ionization yield at the intensities employed in this work. A similar large asymmetry for the high-KER region has also been observed by Wu *et al.* and has been attributed to the ionization of HOMO-2 [4]. Therefore, the ionization pathway for both P2 and P3 at the high intensity (1.5×10^{15} W/cm^2) can be attributed to sequential double ionization from HOMO-2 and HOMO. Meanwhile, it confirms the above identification that P2 and P3 are related to the predissociation of the $1\,^3\Sigma^+$ ($4\sigma^{-1}\,5\sigma^{-1}$) and the $2\,^1\Sigma^+$ ($4\sigma^{-1}\,5\sigma^{-1}$) state, respectively, despite the difference in KER values. By contrast, the MFPADs at the lower intensities [Figs. 4(e) and 4(f), 5(b) and 5(c), and 5(e) and 5(f)] indicate that the CO dication is first populated in the $1\,^1\Sigma^+$ state, after removal of two HOMO electrons. Then a subsequent strong-field-induced excitation is expected to occur from the $1^1\Sigma^+$ state to the $2\,^1\Sigma^+$ state (corresponding to P3) or from the $X\,^3\Pi$ state to the $1\,^3\Sigma^+$ state after the excited $1\,^1\Sigma^+$ state decaying to the $X\,^3\Pi$ state due to their mixing (corresponding to P2), as shown by the dashed red arrows in Fig. 1(d). Finally, these excited states predissociate to produce the peaks with the higher KERs [dotted green and cyan arrows in Fig. 1(d)]. In the study about sequential excitation, Schell *et al.* [17] have shown that, if the photon energy is less than the gap between the excited and the ground states, electronically excited cations are more likely to be created by sequential postionization excitation following the SFI-induced population of the cationic ground state, rather than by a subcycle SFI directly to the cationic excited states [17]. This is in agreement with the low-intensity results in our experiment, where the photon energy (1.55 eV) is lower than the energy gaps between the states involved in the excitation. But this explanation is not applicable to the high-intensity case. As the intensity increases, the ionization probability of HOMO-2 increases substantially, and thus direct SFI from low-lying orbitals become dominant (for the first ionization).

The ionic distributions out of the polarization plane (Fig. 2), which always exist and are similar at the three intensities, can also be understood in terms of the excitation effect. For P1, the maxima perpendicular to the polarization plane [Fig. 2(c)] suggest that these lateral ions come from the $X\,^3\Pi$ state coupling to the impulsive $1\,^3\Sigma^-$ state [43,50]. The production of the $X\,^3\Pi$ state can be attributed to the direct removal of, first, one HOMO-1 electron and, then, one HOMO electron. This results in a much more homogeneous angular distribution than the reverse ionization sequence, as demonstrated by Winney *et al.* [14]. Then the similar distribution for P2 can be understood as being due to postionization excitation from the $X\,^3\Pi$ state to the excited $1\,^3\Sigma^+$ states as well as subsequent predissociation by coupling with the $1\,^3\Sigma^-$ state. Additionally, these analyses also validate the multiple decay and dissociation pathways for the lowest $X\,^3\Pi$ and $1\,^1\Sigma^+$ states and, therefore, explain the observed low yield of the nondissociative CO^{2+} dication.

Even without separating the first and the second electrons, we can resolve the influence of the multiorbital effect. Figure 6 shows the total MFPADs and the relative emission angles between the two electrons, where the two electrons are not distinguished. There is an obvious difference between the low-KER peak P1 and the other two peaks with higher KERs.

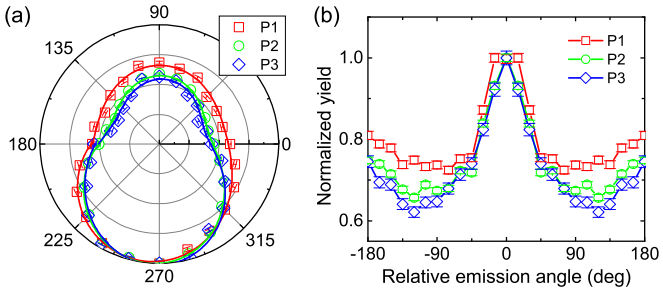

FIG. 6. (a) Total molecular frame angle-dependent ionization yield for the two electrons coincides with the three distinct KER peaks. (b) Relative emission angle between the two electrons in the polarization plane (yz plane) for different peaks. The two electrons are not separated by their ionization orders. The laser intensity is 1.0×10^{15} W/cm^2.

While the MFPADs for P2 and P3 are nearly identical, P1 has MFPADs with lower anisotropies, as shown in Fig. 6(a). The distribution of the relative emission angle between the two electrons, plotted in Fig. 6(b), shows a similar result. These relative angle distributions can also imply the shapes of ionized orbitals and the underlying ionization dynamics of the two electrons. All three curves—for P1, P2, and P3—have two peaks, located at 0° and 180° (−180°). This means that both electrons are emitted either from the same site or from opposite sites, which is consistent with the results presented in Fig. 4. But, in contrast to P2 and P3, the measured data for P1 shown in Fig. 6(b) are distributed more broadly to other angles. This indicates that other molecular orbitals with more homogeneous ionization and electron density angular distribution, such as HOMO-1, are involved in producing the P1-related dissociation, in agreement with the discussion above. Furthermore, it is noteworthy that the measured distribution of the relative angle between two electrons has the potential to reveal the two-electron dynamics including electron correlation in double ionization from the in-depth studies in few-cycle laser fields or in the regime of nonsequential double ionization [14,25].

IV. CONCLUSION

In summary, we have coincidentally measured the KER-resolved angular distribution of ion fragments and the MFPADs for sequential double ionization of the CO molecule with angular streaking. The substantial distributions of ions out of the polarization plane, as well as the KER-dependent total MFPADs and emission angles between the electrons, clearly indicate the involvement of multiple molecular orbitals. By distinguishing the release sequence of the two electrons, the individual MFPAD for each electron, combined with the identification of dissociative dication states, reveals the general participation of low-lying molecular orbitals and the important role of laser-driven excitation for the different pathways of dissociative double ionization of CO. Further comparisons among different intensities suggest that multi-orbital ionization and associated postionization excitation are dependent on the laser intensity. This work verifies the feasibility of using the angular streaking method together with the distinguished MFPADs for each ionization step to investigate the complex ionization, excitation, and dissociation dynamics in strong-field double ionization of molecules. It also sheds some light on the selective control of molecular fragmentation and the studies of electron correlation dynamics.

ACKNOWLEDGMENT

This work was supported by the National Natural Science Foundation of China (NNSFC) (Grants No. 11534004, No. 11704148, and No. 11627807).

[1] H. Akagi, T. Otobe, A. Staudte, A. Shiner, F. Turner, R. Dörner, D. M. Villeneuve, and P. B. Corkum, Science **325**, 1364 (2009).
[2] O. Smirnova, Y. Mairesse, S. Patchkovskii, N. Dudovich, D. Villeneuve, P. Corkum, and M. Y. Ivanov, Nature **460**, 972 (2009).
[3] B. K. McFarland, J. P. Farrell, P. H. Bucksbaum, and M. Guhr, Science **322**, 1232 (2008).
[4] J. Wu, L. P. H. Schmidt, M. Kunitski, M. Meckel, S. Voss, H. Sann, H. Kim, T. Jahnke, A. Czasch, and R. Dörner, Phys. Rev. Lett. **108**, 183001 (2012).
[5] X. Xie, K. Doblhoff-Dier, H. Xu, S. Roither, M. S. Schöffler, D. Kartashov, S. Erattupuzha, T. Rathje, G. G. Paulus, K. Yamanouchi, A. Baltuška, S. Gräfe, and M. Kitzler, Phys. Rev. Lett. **112**, 163003 (2014).
[6] X. Xie, S. Roither, M. Schöffler, E. Lötstedt, D. Kartashov, L. Zhang, G. G. Paulus, A. Iwasaki, A. Baltuška, K. Yamanouchi, and M. Kitzler, Phys. Rev. X **4**, 021005 (2014).
[7] A. E. Boguslavskiy, J. Mikosch, A. Gijsbertsen, M. Spanner, S. Patchkovskii, N. Gador, M. J. J. Vrakking, and A. Stolow, Science **335**, 1336 (2012).
[8] X. M. Tong, Z. X. Zhao, and C. D. Lin, Phys. Rev. A **66**, 033402 (2002).
[9] D. Pavičić, K. F. Lee, D. M. Rayner, P. B. Corkum, and D. M. Villeneuve, Phys. Rev. Lett. **98**, 243001 (2007).
[10] L. Holmegaard, J. L. Hansen, L. Kalhoj, S. L. Kragh, H. Stapelfeldt, F. Filsinger, J. Küpper, G. Meijer, D. Dimitrovski, M. Abu-samha, C. P. J. Martiny, and L. B. Madsen, Nat. Phys. **6**, 428 (2010).
[11] S. Petretti, Y. V. Vanne, A. Saenz, A. Castro, and P. Decleva, Phys. Rev. Lett. **104**, 223001 (2010).
[12] S. Luo, R. Zhu, L. He, W. Hu, X. Li, P. Ma, C. Wang, F. Liu, W. G. Roeterdink, S. Stolte, and D. Ding, Phys. Rev. A **91**, 053408 (2015).
[13] J. Mikosch, A. E. Boguslavskiy, I. Wilkinson, M. Spanner, S. Patchkovskii, and A. Stolow, Phys. Rev. Lett. **110**, 023004 (2013).
[14] A. H. Winney, G. Basnayake, D. A. Debrah, Y. F. Lin, S. K. Lee, P. Hoerner, C. Liao, H. B. Schlegel, and W. Li, J. Phys. Chem. Lett. **9**, 2539 (2018).
[15] S. Luo, S. Zhou, W. Hu, X. Li, P. Ma, J. Yu, R. Zhu, C. Wang, F. Liu, B. Yan, A. Liu, Y. Yang, F. Guo, and D. Ding, Phys. Rev. A **96**, 063415 (2017).
[16] H. Liu, S.-F. Zhao, M. Li, Y. Deng, C. Wu, X.-X. Zhou, Q. Gong, and Y. Liu, Phys. Rev. A **88**, 061401(R) (2013).

[17] F. Schell, A. E. Boguslavskiy, C. P. Schulz, S. Patchkovskii, M. J. J. Vrakking, A. Stolow, and J. Mikosch, Phys. Chem. Chem. Phys. **20**, 14708 (2018).

[18] S. Luo, W. Hu, J. Yu, X. Li, L. He, C. Wang, F. Liu, and D. Ding, J. Phys. Chem. A **121**, 6547 (2017).

[19] S. Luo, S. Zhou, W. Hu, J. Yu, X. Li, P. Ma, L. He, C. Wang, F. Guo, Y. Yang, and D. Ding, J. Phys. Chem. A **122**, 8427 (2018).

[20] P. Sandor, A. Zhao, T. Rozgonyi, and T. Weinacht, J. Phys. B **47**, 124021 (2014).

[21] A. Zhao, P. Sandor, T. Rozgonyi, and T. Weinacht, J. Phys. B **47**, 204023 (2014).

[22] T. Seideman, M. Y. Ivanov, and P. B. Corkum, Phys. Rev. Lett. **75**, 2819 (1995).

[23] J. Zhang, Y. Yang, Z. Li, H. Sun, S. Zhang, and Z. Sun, Phys. Rev. A **98**, 043402 (2018).

[24] A. N. Pfeiffer, C. Cirelli, M. Smolarski, R. Dörner, and U. Keller, Nat. Phys. **7**, 428 (2011).

[25] A. H. Winney, S. K. Lee, Y. F. Lin, Q. Liao, P. Adhikari, G. Basnayake, H. B. Schlegel, and W. Li, Phys. Rev. Lett. **119**, 123201 (2017).

[26] X. Gong, Q. Song, Q. Ji, H. Pan, J. Ding, J. Wu, and H. Zeng, Phys. Rev. Lett. **112**, 243001 (2014).

[27] A. H. Winney, Y. F. Lin, S. K. Lee, P. Adhikari, and W. Li, Phys. Rev. A **93**, 031402(R) (2016).

[28] T. Zuo and A. D. Bandrauk, Phys. Rev. A **52**, R2511 (1995).

[29] H. Xu, E. Loetstedt, A. Iwasaki, and K. Yamanouchi, Nat. Commun. **6**, 8347 (2015).

[30] J. Yao, S. Jiang, W. Chu, B. Zeng, C. Wu, R. Lu, Z. Li, H. Xie, G. Li, C. Yu, Z. Wang, H. Jiang, Q. Gong, and Y. Cheng, Phys. Rev. Lett. **116**, 143007 (2016).

[31] W. Zhang, X. Gong, H. Li, P. Lu, F. Sun, Q. Ji, K. Lin, J. Ma, H. Li, J. Qiang, F. He, and J. Wu, Nat. Commun. **10**, 757 (2019).

[32] E. F. Penka, E. Couture-Bienvenue, and A. D. Bandrauk, Phys. Rev. A **89**, 023414 (2014).

[33] B. Zhang, J. Yuan, and Z. Zhao, Phys. Rev. Lett. **111**, 163001 (2013).

[34] R. Dörner, V. Mergel, O. Jagutzki, L. Spielberger, J. Ullrich, R. Moshammer, and H. Schmidt-Böcking, Phys. Rep. **330**, 95 (2000).

[35] J. Ullrich, R. Moshammer, A. Dorn, R. Dörner, L. P. H. Schmidt, and H. Schmidt-Böcking, Rep. Prog. Phys. **66**, 1463 (2003).

[36] X. Li, C. Wang, Z. Yuan, D. Ye, P. Ma, W. Hu, S. Luo, L. Fu, and D. Ding, Phys. Rev. A **96**, 033416 (2017).

[37] C. Wang, X. Li, X.-R. Xiao, Y. Yang, S. Luo, X. Yu, X. Xu, L.-Y. Peng, Q. Gong, and D. Ding, Phys. Rev. Lett. **122**, 013203 (2019).

[38] K. Henrichs, M. Waitz, F. Trinter, H. Kim, A. Menssen, H. Gassert, H. Sann, T. Jahnke, J. Wu, M. Pitzer, M. Richter, M. S. Schöffler, M. Kunitski, and R. Dörner, Phys. Rev. Lett. **111**, 113003 (2013).

[39] X. Gong, Q. Song, Q. Ji, K. Lin, H. Pan, J. Ding, H. Zeng, and J. Wu, Phys. Rev. Lett. **114**, 163001 (2015).

[40] J. L. Chaloupka, J. Rudati, R. Lafon, P. Agostini, K. C. Kulander, and L. F. DiMauro, Phys. Rev. Lett. **90**, 033002 (2003).

[41] A. Pandey, B. Bapat, and K. R. Shamasundar, J. Chem. Phys. **140**, 034319 (2014).

[42] Z. Wu, C. Wu, X. Liu, Y. Deng, Q. Gong, D. Song, and H. Su, J. Phys. Chem. A **114**, 6751 (2010).

[43] M. Lundqvist, P. Baltzer, D. Edvardsson, L. Karlsson, and B. Wannberg, Phys. Rev. Lett. **75**, 1058 (1995).

[44] A. Talebpour, C. Y. Chien, Y. Liang, S. Larochelle, and S. L. Chin, J. Phys. B **30**, 1721 (1997).

[45] C. Cornaggia and P. Hering, Phys. Rev. A **62**, 023403 (2000).

[46] M. Odenweller, N. Takemoto, A. Vredenborg, K. Cole, K. Pahl, J. Titze, L. P. H. Schmidt, T. Jahnke, R. Dörner, and A. Becker, Phys. Rev. Lett. **107**, 143004 (2011).

[47] P. Eckle, A. N. Pfeiffer, C. Cirelli, A. Staudte, R. Dörner, H. G. Muller, M. Büttiker, and U. Keller, Science **322**, 1525 (2008).

[48] P. Eckle, M. Smolarski, P. Schlup, J. Biegert, A. Staudte, M. Schöffler, H. G. Muller, R. Dörner, and U. Keller, Nat. Phys. **4**, 565 (2008).

[49] N. Camus, E. Yakaboylu, L. Fechner, M. Klaiber, M. Laux, Y. Mi, K. Z. Hatsagortsyan, T. Pfeifer, C. H. Keitel, and R. Moshammer, Phys. Rev. Lett. **119**, 023201 (2017).

[50] T. Šedivcová, P. R. Žd'ánská, V. Špirko, and J. Fišer, J. Chem. Phys. **124**, 214303 (2006).

[51] S. De, M. Magrakvelidze, I. A. Bocharova, D. Ray, W. Cao, I. Znakovskaya, H. Li, Z. Wang, G. Laurent, U. Thumm, M. F. Kling, I. V. Litvinyuk, I. Ben-Itzhak, and C. L. Cocke, Phys. Rev. A **84**, 043410 (2011).

[52] V. S. Prabhudesai, U. Lev, A. Natan, B. D. Bruner, A. Diner, O. Heber, D. Strasser, D. Schwalm, I. Ben-Itzhak, J. J. Hua, B. D. Esry, Y. Silberberg, and D. Zajfman, Phys. Rev. A **81**, 023401 (2010).

[53] D. Pavičić, A. Kiess, T. W. Hansch, and H. Figger, Phys. Rev. Lett. **94**, 163002 (2005).

[54] P. Q. Wang, A. M. Sayler, K. D. Carnes, J. F. Xia, M. A. Smith, B. D. Esry, and I. Ben-Itzhak, Phys. Rev. A **74**, 043411 (2006).